JACS
JOURNAL OF THE AMERICAN CHEMICAL SOCIETY

Communication

pubs.acs.org/JACS

A General Approach to Synthesize Asymmetric Hybrid Nanoparticles by Interfacial Reactions

Jie He,[†] Maria Teresa Perez,[†] Peng Zhang,[‡] Yijing Liu,[†] Taarika Babu,[†] Jinlong Gong,*[,‡] and Zhihong Nie*[,†]

[†]Department of Chemistry and Biochemistry, University of Maryland, College Park, Maryland 20742, United States

[‡]Key Laboratory for Green Chemical Technology of Ministry of Education, School of Chemical Engineering and Technology, Tianjin University, Tianjin 300072, China

Supporting Information

ABSTRACT: Asymmetric multicomponent nanoparticles (AMNPs) offer new opportunities for new-generation materials with improved or new synergetic properties not found in their individual components. There is, however, an urgent need for a synthetic strategy capable of preparing hybrid AMNPs with fine-tuned structural and compositional complexities. Herein, we report a new paradigm for the controllable synthesis of polymer/metal AMNPs with well-controlled size, shape, composition, and morphology by utilizing interfacial polymerization. The hybrid AMNPs display a new level of structural−architectural sophistication, such as controlled domain size and the number of each component of AMNPs. The approach is simple, versatile, cost-effective, and scalable for synthesizing large quantities of AMNPs. Our method may pave a new route to the design and synthesis of advanced breeds of building blocks for functional materials and devices.

The past decade has witnessed tremendous progress in the synthesis of single-component nanoparticles (NPs) with controllable size, shape, and composition.[1,2] However, these NPs would unlikely meet the rising demand for the advanced breeds of building blocks for functional materials and devices.[3−5] Multicomponent NPs with structural and compositional complexities would surpass the inherent limitations imposed on single-component NPs.[6−17] In particular, asymmetric multicomponent nanoparticles (AMNPs) (e.g., dumbbell-like NPs) have shown potential in applications such as sensing,[18] catalysis,[19] self-assembly,[20,21] and nano/opto-electronics.[22,23] Recently, great progress has been achieved in the preparation of pure inorganic AMNPs.[5] In contrast, the synthesis of polymer/inorganic hybrid AMNPs remains a grand challenge. One successful example involves the localized nucleation of polystyrene on the surface of metal or silica NPs to produce Janus type AMNPs using dispersion polymerization.[24,25] This method has significant limitations on producing more complex structures and fine-tuning the dimensions of the products. To date, there has been no report of successful control over the number and dimension of domains in individual polymer/inorganic AMNPs.

This communication describes a simple but versatile strategy for the synthesis of high-quality conjugated polymer−metal AMNPs with fine-tuned morphologies (i.e., lollipop-, dumbbell-, and frog-egg-like) through an interfacial reaction. This approach relies on the diffusion and interfacial reaction of organic monomers and inorganic precursors spatially separated in immiscible organic and aqueous phases. AMNPs can be directly generated in a single step using this approach. The interfacial method allows us to readily control the domain size and the number of each component of AMNPs by tuning the reaction conditions. Dimensions of polymer and metal domains of AMNPs are controllable, ranging from 50 to 180 nm and from 10 to 140 nm, respectively. The ability to utilize the interface in fine-tuning hybrid nanostructures makes our synthetic method conceptually different from others.

In a typical synthesis, organic monomers (e.g., aniline) were dissolved in an organic solvent (e.g., hexane or toluene), while inorganic precursors (e.g., $HAuCl_4$) were dissolved in water with a predetermined concentration.[26] The immiscible solutions were gently placed in a glass vial to form a water−oil interface and incubated at various temperatures overnight. These precursors reacted at the interface for the polymerization of aniline to generate polyaniline (PANi) NPs (denoted as PANPs hereafter) and for the reduction of $HAuCl_4$ to form gold nanoparticles (AuNPs) (see Supporting Information (SI) for details). When the reaction was completed, the aqueous phase was collected and purified by centrifugation. Figure 1a−f show representative TEM images of PANi-Au AMNPs prepared by the interfacial approach with fine-tuned morphologies including lollipop-, dumbbell-, and frog-egg-like shapes, and with a controlled number of Au domains (see more SEM and TEM images in SI, and detailed discussions below). EDX mapping of Au and N elements of AMNPs (Figure 1g) was performed to identify the location of the two components of dumbbell-like AMNPs. The compositional asymmetry of AMNPs can be visually distinguished by the sharp color contrast of Au- and PANi-rich domains. A high resolution TEM image of the Au domain in Figure 1h reveals the polycrystalline structure of AuNPs with multiple twinned boundaries. The Au crystals are mainly composed of (111) planes with a *d*-spacing of 0.235 nm, which is confirmed by a strong diffraction ring of (111) plane in the selected-area electron diffraction (SAED) pattern (Figure 1i inset). The powder X-ray diffraction (XRD)

Received: November 17, 2011
Published: February 9, 2012

   dx.doi.org/10.1021/ja210844h | *J. Am. Chem. Soc.* 2012, 134, 3639−3642

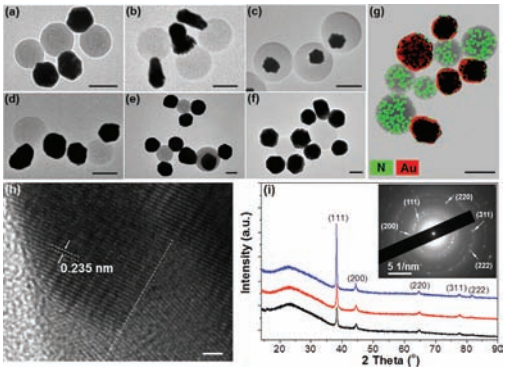

Figure 1. (a–f) TEM images of PANi-Au AMNPs synthesized by the interfacial approach with controlled morphologies (dumbbell (a), lollipop (b), and frog-egg (c)) and a varying number of Au domains (two (d), three (e)) and more (f) Au domains. In TEM images, the black phases are Au, while the gray domains represent PANi. (g) A TEM-EDX mapping of dumbbell PANi-Au AMNPs in (a). The green and red colors represent PANi-rich and Au-rich domains, respectively. (h) A high resolution TEM image of the Au domain of an individual AMNP showing the lattices of Au crystals. The dominant crystal facet (111) has a *d* space of ~0.235 nm. The dash line indicates the twinned boundary. (i) XRD patterns showing the face center cubic crystalline of Au and the amorphous PANi. The inset is an SAED pattern, confirming the polycrystalline structure of Au. The XRD patterns from top to bottom are from dumbbell-, lollipop-, and frog-egg-like AMNPs, respectively. The hump at ~22° (2θ) is attributed to the amorphous PANi phase. Scale bars = 100 nm (a–g) and 2 nm (h).

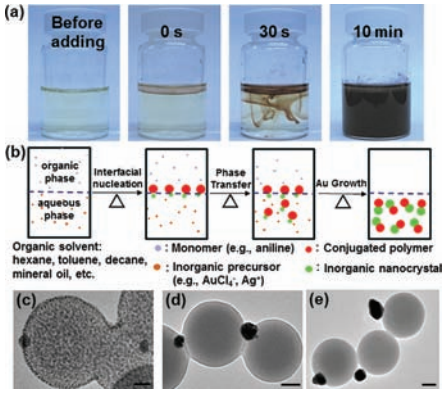

Figure 2. (a) Photographs of a representative interface reaction at different stages. (b) Illustration of the synthetic route involving interfacial nucleation of PANi and Au seeds, and the phase transfer of seeds from the interface to aqueous solution, followed by the continuous growth of Au domains in the aqueous solution. (c–e) TEM images of PANi-Au AMNPs obtained at 5 (c), 20 (d), and 45 min (e) after the reaction. Synthesis condition: 5 mL of 1.4 mM $HAuCl_4$ aqueous solution and 0.5 mL of 20 mM aniline/hexane solution at 45 °C. Scale bars = 20 (c) and 50 nm (d,e).

patterns of AMNPs with different morphologies (Figure 1i) show intensive peaks corresponding to the (111), (200), (220), (311), and (222) Bragg reflections of the cubic crystalline of AuNPs, which is consistent with SAED results. From the diffraction peak at 38° ((111) facet), the size of AuNPs calculated by the Sherrer Equation was 20.6, 17.4, and 31.2 nm for lollipop, frog-egg, and dumbbell AMNPs, respectively. These values are much smaller than the overall Au diameters obtained from TEM,[27] suggesting that each AuNP in AMNPs is composed of multiple single-crystalline Au phases.

Figure 2a shows a series of photographs of typical reaction progress at 0, 0.5, and 10 min. After a brief induction time, two precursors reacted almost immediately at the biphasic interface to initiate the polymerization of aniline and the nucleation of AuNPs; afterward, the resultant NPs proceeded to migrate to the aqueous phase. As schematically illustrated in Figure 2b, we propose the following interface-mediated growth mechanism of AMNPs. Upon establishing the water–oil interface, the oxidation polymerization of aniline monomers is first initiated by $HAuCl_4$ solely at the biphasic interface, resulting in the formation of PANPs. The concomitant reduction of Au(III) to Au(0) simultaneously generates Au nuclei attached on the surface of PANPs. Then, these PANPs with Au nuclei slowly transfer into the aqueous phase as a result of PANi hydrophilicity.[28] Once the initial colloidal NPs depart from the interface, polymerization is terminated due to the cessation of monomer supply. However, residual secondary amine groups in the PANPs can still act as electron donors for the continuous reduction of Au(III) on the Au nuclei, resulting in the further growth of Au domains. This mechanism was confirmed by the time-dependent evolution of AMNP growth. TEM images (Figure 2c–e) show polymer NPs carrying AuNPs obtained at different reaction times. At the initial stage (5 min), only PANPs with minute Au nuclei were formed; the diameter of PANPs was ~120 nm, while that of AuNPs was ~10 nm. The size of AuNPs increased as the reaction proceeded forward and reached up to ~35 nm after 20 min and ~50 nm after 45 min. Note that the diameter of the polymer domain only slightly changed.

The formation of AMNPs was not observed in previous studies or in our control experiments in the absence of the biphasic interface, such as rapidly mixing two aqueous solutions of aniline and $HAuCl_4$ or slowly adding one of the two into the other (see SI).[29–31] In addition, giant free AuNPs (rather than AMNPs) were produced when presynthesized PANPs were added as seeds in a growth solution of gold precursors (see SI). Therefore we deduce that the interface plays a vital role in controlling the nucleation of seeds with particular morphologies by (i) delivering precursors to the interfacial reaction center in a controlled manner and (ii) transferring the formed NPs away from the interface to avoid random formation of PANPs. We notice that the size distribution of Au domains was not obviously broadened by the asynchronous generation of NPs carrying Au nuclei from the interface. The coefficient of variation of AuNPs after overnight reaction was 17.8%. We ascribed the relatively narrow size distribution of Au domains to the focusing effect during the growth process of AuNPs in the aqueous solution.[32]

The kinetics of this interfacial reaction largely depends on the diffusion of all reactants as well as their consumption rate at the interfacial regions. We have systematically investigated the effects of reaction temperature and concentration of each precursor on the formation of AMNPs. The concentration of $HAuCl_4$ (C_{Au}) has a strong impact on both the morphology and size of the synthesized AMNPs (Figure 3). When C_{Au} increased from 0.8 to 1.2 mM, the aspect ratio of Au domains decreased, resulting in a morphological transition of AMNPs from lollipop- to dumbbell-like (Figure 3a,b). To elaborate, lollipop-like AMNPs obtained at C_{Au} = 0.8 mM were composed of a Au "stick" mounted on a spherical PANP (Figure 3a). The dumbbell-like AMNPs synthesized at C_{Au} = 1.2 mM have polyhedral Au domains with an average diameter of 98 nm (Figure 3b). In the studied range of C_{Au}, the average diameter of PANPs increased with increasing C_{Au}, while the size of

dx.doi.org/10.1021/ja210844h | *J. Am. Chem. Soc.* 2012, 134, 3639–3642

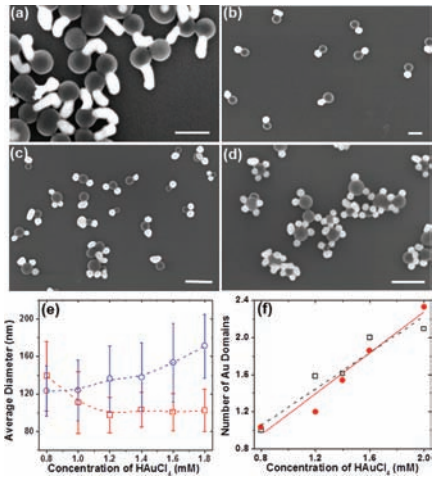

Figure 3. Effect of $HAuCl_4$ concentration on the dimensions and morphologies of AMNPs. (a–d) SEM images of PANi-Au AMNPs obtained at C_{Au} = 0.8 mM, T = 45 °C (a); C_{Au} = 1.2 mM, T = 45 °C (b); C_{Au} = 2.0 mM, T = 45 °C (c); and C_{Au} = 1.4 mM, T = 60 °C (d). 0.5 mL of 20 mM aniline in hexane was used in all the reactions. The average number of Au domains in individual AMNP is 1.04 (a), 1.18 (b), 2.30 (c), and 3.75 (d). (e) The average diameter of AuNPs (□) and PANPs (○) plotted as a function of C_{Au}. Each point in (e) was obtained by averaging more than 100 NPs. (f) The average number of Au domains on each AMNP obtained from SEM measurements (●) and theoretical calculation (□) plotted as a function of C_{Au}. Each point in (f) was obtained by averaging 250 NPs. Scale bars = 200 nm (a–b) and 400 nm (c–d).

AuNPs slightly decreased with C_{Au} (Figure 3e). A further increase of C_{Au} above 1.2 mM led to an increase in the average number of Au domains (N_{Au}) on single PANPs, while the size of each AuNP roughly remained constant (Figure 3c). Figure 3f shows that N_{Au} on a single PANP increases linearly as a function of C_{Au}, approximately in agreement with theoretical calculation based on the mass conversation law (see SI for calculations). At C_{Au} = 2.0 mM, the average number of Au domains on each AMNP increased up to 2.30.

As mentioned earlier on, fine-tuning the relative size and number of multicomponent domains in individual NPs remains a challenge. So far, AMNPs with multiple domains have been rarely reported.[17] One example of crystalline NPs is Au-(n)Fe_3O_4 and Fe_3O_4-(n)Ag, where n represents the number of multiple domains.[7,10] Compared to the solvothermal synthesis of heterogeneous pure inorganic nanocrystals, the formation of multiple Au domains in our system could be attributed to the interplay of the diffusion rate of each precursor and the rate of polymerization (υ) occurring at the interface. As $C_{Ani} \geq 10C_{Au}$, we assume that υ is limited by the diffusion of $HAuCl_4$ toward the interfacial region;[33] that is, $\upsilon \propto C_{Au}^{0.5} \times C_{Ani}^{1.5} \propto D \times \nabla C_{Au} \times C_{Ani}^{1.5}$, where D and ∇C_{Au} are the diffusion coefficient and the gradient of $HAuCl_4$ normal to the interface due to its consumption in reaction, respectively. Higher C_{Au} gives a larger ∇C_{Au} that increases υ, but the nucleation rate of AuNPs at the interfacial region somehow increases faster than υ, thus leading to a larger N_{Au} on one PANP.[33]

The reaction temperature (T) strongly affects the interfacial synthesis as well. Interestingly, the generation of AMNPs only occurred at $T \geq 40$ °C. Below 40 °C, the formation of AMNPs was suppressed, and PANi-Au nanocomposites with ~10-nm-diameter AuNPs were produced (see SI). A possible explanation is that a slower reaction at lower temperature leads to the diffusion of aniline unconsumed at the interfacial region into the aqueous phase, where the homogeneous reaction in the aqueous phase disfavored the formation of AMNPs.[29,30] As a result, temperature becomes another factor in tuning the N_{Au} of AMNP: increasing T would increase N_{Au}. Figure 3d shows representative AMNPs with multiple Au domains (N_{Au} is up to 3.75) on each PANP prepared at 60 °C. The possible reason for the increased Au domains is the much stronger oxidizability of $HAuCl_4$ and thus a faster nucleation of AuNPs at a higher temperature.

The concentration of aniline also plays an important role in controlling the dimensions and morphologies of AMNPs (Figure 4). With increasing C_{Ani}, a morphological transition

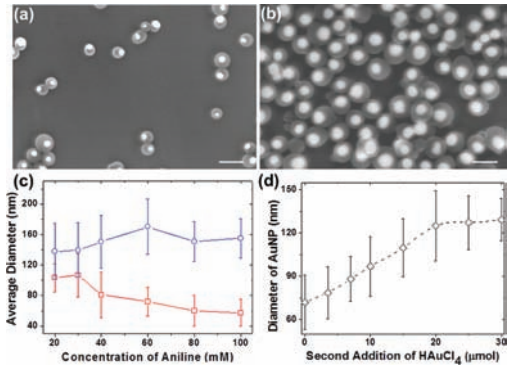

Figure 4. Effect of C_{Ani} on dimensions and morphologies of AMNPs. (a) SEM image of AMNPs obtained using 0.5 mL of 20 mM aniline. The reaction was performed with 5 mL of 1.4 mM $HAuCl_4$ aqueous solution at 45 °C. (b) SEM image of AMNPs obtained by further adding 20 μmol of $HAuCl_4$ in (a) solution. (c) The average diameter of AuNPs (□) and PANPs (○) plotted as a function of C_{Ani}. Each point in (c) was obtained by averaging over 100 particles. (d) The average size of AuNPs plotted as a function of the secondary addition of $HAuCl_4$. Scale bars = 250 nm.

from dumbbell- to frog-egg-like AMNPs was observed (Figure 4a and SI). In the range of aniline concentrations studied, once the generation of AuNPs is equilibrated with that of PANPs, the process will lead to the generation of frog-egg-like NPs. Compared to dumbbell NPs, only one single AuNP was present on each individual frog-egg-like AMNP with ~100% yield. As $\upsilon \propto C_{Ani}^{1.5}$, υ at a higher C_{Ani} prevails over the rate of formation of AuNPs, resulting in PANPs without any attached AuNPs (see SI). This result further supported our interpretation of the interfacial reaction mechanism.

We observed that the AuNPs can continue to grow dynamically upon further addition of $HAuCl_4$ into the AMNPs (Figure 4b). The size of Au domains increased linearly with increasing C_{Au} during the subsequent addition (Figure 4d), which is a characteristic of a living reaction. These results indicate the following: (i) the surface of AuNPs is not covered with polymer and it is possible for additional selective surface modification as needed, which also further distinguished our method from the others;[24,25] (2) the final size of AuNPs can be fine-tuned on demand; and (3) more complex AMNPs can be developed by sequentially depositing other metals.

The effect of aniline and $HAuCl_4$ concentrations on the synthesis of AMNPs was summarized in a product diagram in Figure 5. At C_{Ani} < 10 mM, the formation of AMNPs was suppressed across the studied range of C_{Au}, presumably due to the low polymerization rate of PANPs to initiate the growth of

dx.doi.org/10.1021/ja210844h | J. Am. Chem. Soc. 2012, 134, 3639–3642

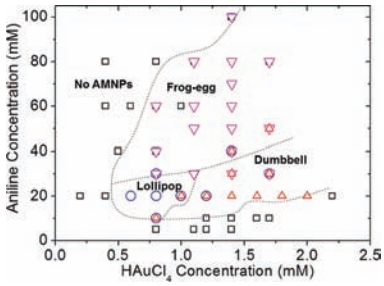

Figure 5. Product diagram summarizing the effect of C_{Au} and C_{Ani} on the synthesis of AMNPs at 45 °C. The dashed lines indicate the superimposed boundaries between different morphological regions of AMNPs: no AMNPs (□); lollipop (○); dumbbell (Δ); frog-egg (∇).

AMNPs. In this case, PANPs randomly covered with a large amount of small AuNPs (~10 nm) were obtained (see SI). At 10 mM < C_{ani} < 30 mM, lollipop-like AMNPs were synthesized in a narrow window of C_{Au} (0.6−1.0 mM), while the dumbbell-like AMNPs with a controlled number of Au domains were obtained at C_{Au} > 1.0 mM. At C_{Ani} > 30 mM, the frog-egg-like AMNPs were the dominant products in a wide C_{Au} range.

In conclusion, we have developed a new yet simple paradigm to synthesize a diverse range of hierarchical AMNPs with controlled morphologies. This synthesis can be easily scaled up to large quantities. To the best of our knowledge, this is the first report on the synthesis of polymer/inorganic AMNPs using two-phasic reactions. We have also identified a new interfacial-mediated mechanism for the synthesis of AMNPs, which distinguishes our synthetic method from others.[24,25] This biphasic approach could also be used to synthesize other types of polymer/inorganic or inorganic/inorganic AMNPs. Our approach offers overall exquisite reproducibility and precision in tuning the nanoscale domains in AMNPs, which is essential in applications such as sensing, catalysis, and optoelectronic devices. In particular, AMNPs with multiple interaction sites can serve as novel building blocks for directional or programmable self-assembly of new functional materials and devices.[3] This work constitutes an important step toward bottom-up synthesis of complex multicomponent nanostructures with desired morphologies and properties.

■ ASSOCIATED CONTENT

Supporting Information

The detailed synthesis condition, characterization, and other SEM/TEM images. This material is available free of charge via the Internet at http://pubs.acs.org.

■ AUTHOR INFORMATION

Corresponding Author

jlgong@tju.edu.cn; znie@umd.edu

Notes

The authors declare no competing financial interest.

■ ACKNOWLEDGMENTS

This work is supported by startup funds from the University of Maryland, NSFC (21006068) and Program of Introducing Talents of Discipline to Universities (B06006). We thank Prof. Amy S. Mullin for helpful discussions, Dr. Xiaogang Han for help on electrochemical characterization, and Dr. Li-Chung Lai for assistance on TEM imaging. We acknowledge the support of Maryland NanoCenter and its NispLab. The NispLab is supported in part by the NSF as an MRSEC Shared Experimental Facilities.

■ REFERENCES

(1) Xia, Y. N.; Yang, P. D.; Sun, Y. G.; Wu, Y. Y.; Mayers, B.; Gates, B.; Yin, Y. D.; Kim, F.; Yan, Y. Q. *Adv. Mater.* **2003**, *15*, 353.
(2) Perez-Juste, J.; Pastoriza-Santos, I.; Liz-Marzan, L. M.; Mulvaney, P. *Coord. Chem. Rev.* **2005**, *249*, 1870.
(3) Glotzer, S. C.; Solomon, M. J. *Nat. Mater.* **2007**, *6*, 557.
(4) Nie, Z. H.; Petukhova, A.; Kumacheva, E. *Nat. Nanotechnol.* **2010**, *5*, 15.
(5) Carbone, L.; Cozzoli, P. D. *Nano Today* **2010**, *5*, 449.
(6) Teranishi, T.; Inoue, Y.; Nakaya, M.; Oumi, Y.; Sano, T. *J. Am. Chem. Soc.* **2004**, *126*, 9914.
(7) Yu, H.; Chen, M.; Rice, P. M.; Wang, S. X.; White, R. L.; Sun, S. H. *Nano Lett.* **2005**, *5*, 379.
(8) Kwon, K. W.; Shim, M. *J. Am. Chem. Soc.* **2005**, *127*, 10269.
(9) Shi, W. L.; Zeng, H.; Sahoo, Y.; Ohulchanskyy, T. Y.; Ding, Y.; Wang, Z. L.; Swihart, M.; Prasad, P. N. *Nano Lett.* **2006**, *6*, 875.
(10) Choi, J. S.; Jun, Y. W.; Yeon, S. I.; Kim, H. C.; Shin, J. S.; Cheon, J. *J. Am. Chem. Soc.* **2006**, *128*, 15982.
(11) Wei, Y. H.; Klajn, R.; Pinchuk, A. O.; Grzybowski, B. A. *Small* **2008**, *4*, 1635.
(12) Jiang, S.; Chen, Q.; Tripathy, M.; Luijten, E.; Schweizer, K. S.; Granick, S. *Adv. Mater.* **2010**, *22*, 1060.
(13) Xing, S. X.; Feng, Y. H.; Tay, Y. Y.; Chen, T.; Xu, J.; Pan, M.; He, J. T.; Hng, H. H.; Yan, Q. Y.; Chen, H. Y. *J. Am. Chem. Soc.* **2010**, *132*, 9537.
(14) Chen, T.; Chen, G.; Xing, S. X.; Wu, T.; Chen, H. Y. *Chem. Mater.* **2010**, *22*, 3826.
(15) Zou, H. Y.; Yan, D. Q.; Mohi, G. *FEBS Lett.* **2011**, *585*, 1007.
(16) Peng, S.; Lei, C. H.; Ren, Y.; Cook, R. E.; Sun, Y. G. *Angew. Chem., Int. Ed.* **2011**, *50*, 3158.
(17) Costi, R.; Saunders, A. E.; Banin, U. *Angew. Chem., Int. Ed.* **2010**, *49*, 4878.
(18) Hao, R.; Xing, R. J.; Xu, Z. C.; Hou, Y. L.; Gao, S.; Sun, S. H. *Adv. Mater.* **2010**, *22*, 2729.
(19) Crossley, S.; Faria, J.; Shen, M.; Resasco, D. E. *Science* **2010**, *327*, 68.
(20) Glaser, N.; Adams, D. J.; Boker, A.; Krausch, G. *Langmuir* **2006**, *22*, 5227.
(21) He, J.; Hourwitz, M. J.; Liu, Y.; Perez, M. T.; Nie, Z. *Chem Commun* **2011**, *47*, 12450.
(22) Gangwal, S.; Cayre, O. J.; Velev, O. D. *Langmuir* **2008**, *24*, 13312.
(23) Nisisako, T.; Torii, T.; Takahashi, T.; Takizawa, Y. *Adv. Mater.* **2006**, *18*, 1152.
(24) Ohnuma, A.; Cho, E. C.; Camargo, P. H. C.; Au, L.; Ohtani, B.; Xia, Y. N. *J. Am. Chem. Soc.* **2009**, *131*, 1352.
(25) Perro, A.; Reculusa, S.; Pereira, F.; Delville, M. H.; Mingotaud, C.; Duguet, E.; Bourgeat-Lami, E.; Ravaine, S. *Chem. Commun.* **2005**, 5542.
(26) Huang, J. X.; Virji, S.; Weiller, B. H.; Kaner, R. B. *J. Am. Chem. Soc.* **2003**, *125*, 314.
(27) Borchert, H.; Shevehenko, E. V.; Robert, A.; Mekis, I.; Kornowski, A.; Grubel, G.; Weller, H. *Langmuir* **2005**, *21*, 1931.
(28) Zhong, W. B.; Chen, X. H.; Liu, S. M.; Wang, Y. X.; Yang, W. T. *Macromol. Rapid Commun.* **2006**, *27*, 563.
(29) Guo, Z. R.; Zhang, Y.; DuanMu, Y.; Xu, L.; Xie, S. L.; Gu, N. *Colloids Surf., A* **2006**, *278*, 33.
(30) Zhang, L.; Peng, H.; Kilmartin, P. A.; Soeller, C.; Tilley, R.; Travas-Seidic, J. *Macromol. Rapid Commun.* **2008**, *29*, 598.
(31) Wang, Z. J.; Yuan, J. H.; Han, D. X.; Niu, L.; Ivaska, A. *Nanotechnology* **2007**, *18*, 115610.
(32) Peng, X. G.; Wickham, J.; Alivisatos, A. P. *J. Am. Chem. Soc.* **1998**, *120*, 5343.
(33) Qiu, W.; Huang, H. A.; Zeng, S.; Xue, T.; Liu, J. X. *J. Polym. Res.* **2011**, *18*, 19.